Algorithmic Operations Research

Optimizing the gVERSE RF Pulse Sequence:
An Evaluation of Two Competitive Software Algorithms

Christopher K. Anand, Stephen J. Stoyan et Tamás Terlaky

Résumé de l'article

Radio Frequency (RF) pulses cause elevated patient temperatures during Magnetic Resonance Imaging (MRI) procedures. Generalized Variable Rate Selective Excitation (gVERSE) is a co-design method for Radio Frequency (RF) pulse and slice gradient which minimizes Specific Absorption Rate (SAR) (the accepted predictor of patient heating). After developing a rigorous mathematical model, the nonlinear gVERSE optimization problem is solved using two competitive software packages. The gVERSE solutions generated by Sparse Optimal Control Software (SOCS) and AMPL–MINOS produce two separate variations of SAR reducing pulses. The different software solutions are compared using numerical simulations of slice selection. The computational experiments involved with the gVERSE model provided insight towards using different software to solve highly demanding mathematical optimization problems.

Optimizing the gVERSE RF Pulse Sequence: An Evaluation of Two Competitive Software Algorithms

Christopher K. Anand [a] Stephen J. Stoyan [b] Tamás Terlaky [c,1]

[a]Department of Computing and Software, School of Computational Engineering and Science, McMaster University, Hamilton, ON, Canada.
[b]Department of Mechanical and Industrial Engineering, University of Toronto, ON, Canada
[c]Department of Industrial and Systems Engineering, Lehigh University, Bethlehem, PA, USA

Abstract

Radio Frequency (RF) pulses cause elevated patient temperatures during Magnetic Resonance Imaging (MRI) procedures. Generalized Variable Rate Selective Excitation (gVERSE) is a co-design method for Radio Frequency (RF) pulse and slice gradient which minimizes Specific Absorption Rate (SAR) (the accepted predictor of patient heating). After developing a rigorous mathematical model, the nonlinear gVERSE optimization problem is solved using two competitive software packages. The gVERSE solutions generated by Sparse Optimal Control Software (SOCS) and AMPL–MINOS produce two separate variations of SAR reducing pulses. The different software solutions are compared using numerical simulations of slice selection. The computational experiments involved with the gVERSE model provided insight towards using different software to solve highly demanding mathematical optimization problems.

Key words: RF pulse sequence, gVERSE, MRI, voxel, nonlinear programming, SOCS, optimal control.

1. Introduction

Over the past decade Magnetic Resonance Imaging (MRI) has had a profound impact on health care. Today, many hospitals, sports clinics, and other types of health facilities own or share the use of an MRI machine. The machines provide high resolution cross-sectional diagnostic images of various parts of the body. The MRI machines operate by sending a selective Radio Frequency (RF) pulse through a large magnet that is accompanied by field gradients. The RF pulse and gradient waveform are know as the RF pulse sequence and they are responsible for producing a signal that is transformed into the final image [12]. Recently, many RF pulse sequences, or selective excitations, have been designed that each have advantages and disadvantages with respect to image quality, speed, safety, etc. One important element of RF pulse sequences is the level of SAR (Specific Absorption Rate) produced during excitations. During MRI procedures high levels of SAR can cause undesired side effects such as skin burns. This is the focus of the gVERSE pulse, producing useable

MR (Magnetic Resonance) signals while minimizing patient SAR levels. The gVERSE pulse is generated using a novel nonlinear optimization approach, which is novel in allowing arbitrary changes in both RF and gradient waveforms. The nonlinear program is captured in an optimal control framework, and presented to SOCS, a solver adpated to optimal control problems. The problem is also formulated as a general nonlinear program (NLP) for the purposes of comparing SOCS solutions to solutions provided by a general solver, MINOS in this case.

With regards to RF pulse sequences, several researchers have employed different optimization methods in their designs. Some of the most common are: quadratic optimization [7], evolutionary algorithms [17], simulated annealing [14], and optimal control techniques [6,16]. However, most approaches are computationally intensive and in many cases their design for the pulse-envelope consists of relaxed conditions to meet their desired profile. The optimal control approach in [16] seems to be the most promising, yet, the models transform the Bloch equation into the Chebyshev domain leading to an ill-conditioned algebraic problem. Conolly *et al.* (1986) designed the first ver-

sion of the Variable Rate Selective Excitation (VERSE) pulse, which is aimed at reducing MRI SAR levels. Several years later, Conolly and other collaborators used VERSE pulses to minimize the duration of excitation by increasing both RF and gradient amplitudes, [8]. In this paper we define the generalized VERSE (gVERSE) pulse, which uses Conolly's *et al.* original idea but is expressed in a dynamic nonlinear optimization setting that is directly aimed at reducing RF SAR levels. The gVERSE pulse is a highly selective pulse that differs from the VERSE pulse with respect to how SAR is minimized. As well, the dynamics of the problem are significantly increased by the addition of restrictive constraints and enhanced degrees of freedom [1,15]. We present two RF pulse sequences as a background to the optimization method that was used to solve the gVERSE pulse. This investigation highlights two different solution techniques used in solving the gVERSE NLP problem and compares the validity of their solutions.

This paper is organized as follows: we begin with an overview of general RF pulse sequences and the VERSE pulse model presented in [7]. In Section 3, the gVERSE model is defined with the final NLP problem and discretizations. The implementation issues involved in computing the gVERSE pulse are described in Section 4. Sparse Optimal Control Software (SOCS) and AMPL–MINOS are used to solve the gVERSE problem, important functionality issues are discussed in this section. In Section 5, the computational results for the gVERSE pulse are shown for the two different test cases. The results are graphically illustrated and the software performance is further tested using an MRI simulation. Finally, we conclude on the different solutions generated by the softwares and illustrate how not only optimization, but optimization software, can have a profound effect on improving RF pulse sequences.

2. RF Pulse Background

We begin with a basic review of MRI mathematics and present the motivation and functionality of two different types of RF pulse sequences. For more information the reader can refer to [5,11,12]. In the most basic sense, an MRI alters a specimens (or objects) magnetic field to obtain a reading that eventually produces an image. The Bloch equation provides the rate of magnetization ($d\overrightarrow{M}(t)/dt$) of a specimen

$$\frac{d\overrightarrow{M}(t)}{dt} = \gamma \overrightarrow{M}(t) \times \overrightarrow{B}(t) + \frac{1}{\tau_1}(M_0 - M_z(t))\widehat{z}$$
$$- \frac{1}{\tau_2}\overrightarrow{M}_\perp(t),$$

where t is time, $\overrightarrow{B}(t)$ is the external magnetic field in the z-axis direction, γ is the gyromagnetic constant, and

$$\overrightarrow{M}(t) = \begin{bmatrix} M_x(t) \\ M_y(t) \\ M_z(t) \end{bmatrix}, \text{ and } \overrightarrow{M}_\perp(t) = \begin{bmatrix} M_x(t) \\ M_y(t) \\ 0 \end{bmatrix}$$

are the net and transverse magnetization vectors, respectively. In addition, $\widehat{z}$ is the z-axis unit vector, M_0 is the initial magnetization in the $\widehat{z}$ direction, τ_1 is the spin-lattice and τ_2 is the spin-spin interaction parameters. For our computations, we define

$$\overrightarrow{B}(t) = \begin{bmatrix} b_x(t) \\ b_y(t) \\ b_z(t) \end{bmatrix},$$

where $b_x(t)$, $b_y(t)$, and $b_z(t)$ are the external magnetization vector coordinates. The basics MRI functionality are as follows: (a) first a specimen is placed in a large magnet and magnetized. This causes the magnetization vectors (net spin of hydrogen nuclei) in the specimen to "line up" and point in the same direction, called the direction of the external magnetic field. (b) The RF pluse sequence is applied to the specimen. The RF pulse tips some of the magnetization vectors into what is called the transverse plane, which is perpendicular to the direction of the external field, and a signal is given off. The accompanying gradient waveform alters the signal by modulating the phase of the magnetization as a function of posiiton. (c) The signal is stored and combined with other MR signals and transformed into an image. This is a general description of how an RF pulse sequence generates a useable MR signal, for a detailed analysis of this process one can look at [10–12,15].

2.1. *Generic RF Pulse Sequence*

To process an MR image, a number of precise RF pulses are applied in combination with synchronized gradients in different directions. As mentioned, the RF pulse and gradient waveform make up the RF pulse sequence, in which a signal for imaging is generated. RF pulses are only designed to excite a specific portion of the object or specimen that the user intends to image, although, both the RF and gradient waveforms interact with the whole object. In the case of slice excitation,
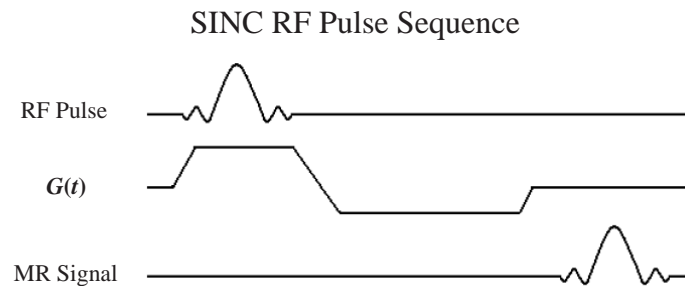
SINC RF Pulse Sequence

Fig. 1. A typical SINC pulse imaging sequence.

the gradient is restricted to a single direction, in contrast to the case of readout gradients, which are used to spatially modulate the signal, [5]. There are many different types of RF and gradient waveform combinations that generate useable signals. Gaussian and SINC pulses are just two examples of the various RF pulse sequences used today. Figure 1 provides an illustration of a slice select SINC pulse sequence [11]. These and most more sophisticated pulses currently used hold the gradient waveform constant during the RF excitation. Although SINC pulse sequences are successful at exciting particular magnetization vectors into the transverse plane, they fail to account for side effects such as SAR levels. The level of SAR is directly related to the heating effect experienced by patients during MRI procedures. This is a result of the RF pulse used and becomes particularly important with pediatric patients. For this reason the FDA has strict limitations on SAR, which subsequently restricts RF pulse potential and other elements involved in MRI procedures. With regards to MRI systems, the RF pulse sequence is one area that tends to be a bottle neck. Researchers are developing faster scanners, higher field magnets, enhanced software components, and improved RF coils; however, they are still limited by SAR levels produced by current RF pulse sequences.

2.2. *The VERSE Pulse Sequence*

As defined in [8], VERSE is a technique that uses a time-varying gradient to change the shape of the RF pulse without changing the spatial excitation profile on resonance. Originally proposed by Conolly *et al.* in 1986, VERSE pluses generate MR signals similar to generic RF pulses while reducing SAR levels via differential time scaling. As mentioned, the SAR of a selec-

tive RF pulse is a critical parameter in clinical settings and may limit the use of a particular pulse sequence if the SAR limit exceeds given FDA requirements [12]. Due to the high SAR levels of various RF pluses the scan time for given pulse sequences are restricted, which contributes to the overall time of MRI procedures [7]. The VERSE pulse provides a trade-off between time and amplitude that allows the duration of the pulse to be extended [7]. As shown in Figure 2, VERSE pulses contain a flattened center peak and their gradient waveform posses two additional steps. The uniform redistribution of the pulse area allows for a decrease in the level of SAR. Conolly *et al.* (1986) designed three different types of SAR reducing VERSE pulses. The first model consisted of a minimum–SAR facsimile pulse, whereby for a specified duration the gradient waveform and RF pulse were integrated in the objective and subject to maximum gradient and constant duration constraints. The second model used a minimum time formulation approach, whereby it searched for the smallest pulse that would generate a signal, which was constrained by an RF amplitude and gradient upper bound. The parametric gradient was the final model presented by Conolly *et al.*, it was constrained by both the maximum gradient and slew-rate, and involved the parametric gradient and the RF pulse in the objective function. The first two models contained $3\kappa+1$ variables, where κ was the total number of samples or RF pulses. The third model, the parametric gradient, contained $\kappa(p + 1) + 1$ variables, where p represents the dimension of a parameter vector. For their results, a total of 256 sample values were used, which kept the variable count relatively low [7]. Of the three algorithms, the parametric formulation offered the best SAR reduction, however, the design still had areas for improvement as the results contained gradient and RF timing mismatches. Although further experimenta-
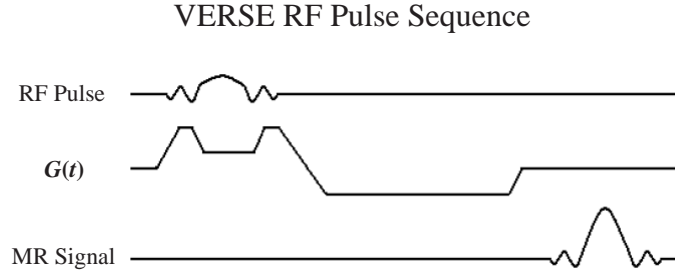
VERSE RF Pulse Sequence

Fig. 2. The VERSE pulse imaging sequence.

tion was necessary, Conolly *et al.* (1986) were the first to motivate this innovative concept.

3. The gVERSE Pulse Sequence

The generalized VERSE (gVERSE) pulse is designed to further minimize RF pulse amplitudes and SAR levels over that of its VERSE predecessor. Conolly *et al.* (1986) provide evidence that SAR can be reduced by combined RF/gradient reductions and time dilations. An idea of the gVERSE pulse is illustrated in Figure 3, for more information the reader may refer to [1,15]. Our aim is to lower RF pulse energy and evenly distribute the pulse signal. This equates to searching for a larger parameter space by allowing arbitrary gradient waveforms (subject to machine constraints), including sign changes. By convention, the flattened RF pulse shown in Figure 3 will allow for a longer signal reading and a decrease in the level of SAR. Mathematically, this equates to minimizing the energy of the external magnetic field generated by the RF pulse ($\overrightarrow{B}_{\mathrm{rf}}(t)$), and therefore our objective is

$$\min \text{ SAR} = \int_0^T |\overrightarrow{B}_{\mathrm{rf}}(t)|^2 dt = \int_0^T b_x^2(t) + b_y^2(t) dt, \quad (1)$$

where T is the time at the end of the RF pulse and

$$\overrightarrow{B}_{\mathrm{rf}}(t) = \begin{bmatrix} b_x(t) \\ b_y(t) \\ 0 \end{bmatrix}.$$

MRI is based on the interaction of nuclear spin with an external magnetic field, hence, $\overrightarrow{B}_{\mathrm{rf}}(t)$ is the vertical and horizontal components of $\overrightarrow{B}(t)$. Also note that if low pulse amplitudes are produced by the gVERSE pulse then the duration, T, of the pulse can be increased.

Since all magnetization vectors are spinning in the same direction, a product of the large magnet over the specimen, there exists a rotational frame of reference. We set up our equations in the rotating frame of reference to exclude the uniform magnetic field generated by the main super-conducting magnet, B_0. Thus, we are left with the magnetic field present in the RF pulse, $\overrightarrow{B}_{\mathrm{rf}}(t)$, and our gradient

$$\overrightarrow{G}(t, s) = \begin{bmatrix} 0 \\ 0 \\ sG(t) \end{bmatrix},$$

where $sG(t)$ is the gradient value at coordinate position s, which we define in the $\hat{z}$ direction. As mentioned at the start of this section, the primary function of the gradient is to produce a temporally and spatially varying magnetic field such that the MR signal can be spatially modulated [11]. Therefore, by changing the gradient field strength, different parts of a specimen experience different field values as a function of their spatial coordinate position. By multiplying a constant gradient value by different coordinate positions s, we observe a linear relationship. Designing gradients to produce uniformly linear fields is another interesting design optimization problem in MRI. For our analysis, coordinate positions s split a specimen (or object) into planes or "slices" along the $\hat{z}$ direction, as illustrated in Figure 4. The coordinate position s measures the position in what is usually called the "slice" direction, and in single slice imaging, the external magnetic field at a point is always a function of s and time alone. The example pulses in this paper seek to excite specified magnetization vectors into the transverse (x, y) plane. This is not a restriction of the model or software, but it simplifies the explanation. In MRI a voxel corresponds to a unit volume of protons which together produce a pixel of graphic information [11], and as this is directly
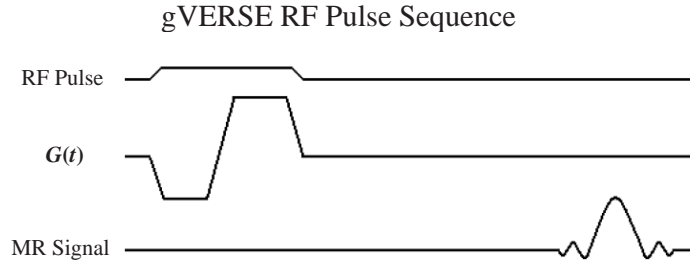
gVERSE RF Pulse Sequence
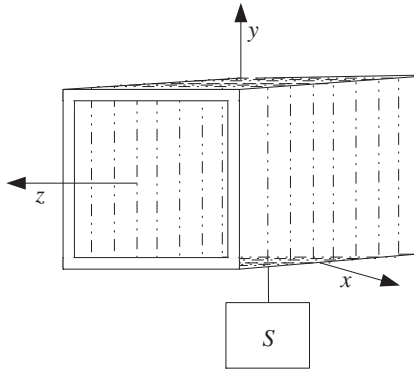

Fig. 3. The gVERSE pulse imaging sequence.

Fig. 4. Specimen (or object) separated into slices across the z-axis.

related to a group or unit volume of magnetization vectors, for our analysis we will use the word voxel and magnetization vector interchangeably. Thus, s allows us to distinguish between voxels that are excited into the transverse plane and those that are not. Note that in order to obtain a useable signal some of the voxels are tipped into the transverse plane and others point in the direction of the external magnetic field, B_0. Coordinate positions s of voxels that are excited into the transverse plane will be referred to as being "in the slice." Magnetization vectors that are not tipped into the transverse plane, which remain in the direction of B_0, will be referred to as being "outside the slice." Given the set of all coordinate positions $s \in S$ we divide the voxels that are in the slice and outside the slice. Thus, let S_{in} represent the set of coordinate positions s in the slice and S_{out} represent the set of positions s that are outside the slice. Then S becomes the disjoint union of the sets $S_{\text{in}} \cup S_{\text{out}}$, where $S \in \mathbb{R}$. In practice, the image area of any specimen (or object) that a signal is generated will have a fixed length, S_{in}

represents this area. Thus, for each coordinate position $s \in S$ we add constraints corresponding to the Bloch equation, however, boundary constraints correspond to different conditions depending on the position of the slice. Voxels $s \in S_{\text{in}}$ uniformly tip into the transverse plane, whereas voxels $s \in S_{\text{out}}$ certify that external magnetization is preserved.

Expressing the magnetic field $\overrightarrow{B}(t,s)$ with respect to coordinate positions s, whereby $b_x(t)$ and $b_y(t)$ are independent of s, we have

$$\overrightarrow{B}(t,s) = \overrightarrow{B}_{\text{rf}}(t) + \overrightarrow{G}(t,s).$$

Also, since $\overrightarrow{B}(t,s)$ has divided the $\widehat{z}$ component of our external magnetization into coordinate components, the same notation is introduced to our net magnetization vector. Therefore, we have

$$\overrightarrow{M}(t,s) = \begin{bmatrix} M_x(t,s) \\ M_y(t,s) \\ M_z(t,s) \end{bmatrix}.$$

As VERSE pulses typically have short sampling times we will assume the same for the gVERSE pulse leaving proton interactions and relaxation out of the formulations. Therefore, including positions s into the Bloch equation we have

$$\frac{d\overrightarrow{M}(t,s)}{dt} = \gamma \overrightarrow{M}(t,s) \times \overrightarrow{B}(t,s),$$

which expands to

$$\overrightarrow{M}(t,s) \times \overrightarrow{B}(t,s) =$$
$$\begin{bmatrix} 0 & -sG(t) & b_y(t) \\ sG(t) & 0 & -b_x(t) \\ -b_y(t) & b_x(t) & 0 \end{bmatrix} \begin{bmatrix} M_x(t,s) \\ M_y(t,s) \\ M_z(t,s) \end{bmatrix},$$

and finally

$$\frac{d\overrightarrow{M}(t,s)}{dt} = \gamma \begin{bmatrix} 0 & -sG(t) & b_y(t) \\ sG(t) & 0 & -b_x(t) \\ -b_y(t) & b_x(t) & 0 \end{bmatrix} \overrightarrow{M}(t,s). \tag{2}$$

Under practical situations, when stimulating a segment of a specimen by an RF pulse some of the magnetization vectors are fully tipped into the transverse plane, partially tipped, and those lying outside the slice profile are minimally affected. The second case, pertains to magnetization vectors that are only partially tipped into the transverse plane. These voxels are described as having off-resonance and tend to disrupt pulse sequences and distort the final MR image [11]. In anticipation of removing such in-homogeneities we introduce two constraints to the model that allows the final position of the magnetization vectors to be in the direction of the transverse plane or the external magnetic field. Using an angle α, the net magnetization of the voxels in S_{in} from the $\widehat{z}$ direction to the transverse plane are defined. By convention, α will be the greatest at the end of our RF pulse, at time T, and since we are in the rotating frame we can remove the y-axis from our equations. Thus, we eliminate off-resonance s coordinates by bounding S_{in} voxels affected by the pulse in

$$\left\| \begin{bmatrix} M_0\sin(\alpha) \\ 0 \\ M_0\cos(\alpha) \end{bmatrix} - \begin{bmatrix} M_x(T,s) \\ M_y(T,s) \\ M_z(T,s) \end{bmatrix} \right\| \le \varepsilon_1, \tag{3}$$

and those in S_{out} ($\alpha = 0$)

$$\left\| \begin{bmatrix} 0 \\ 0 \\ M_0 \end{bmatrix} - \begin{bmatrix} M_x(T,s) \\ M_y(T,s) \\ M_z(T,s) \end{bmatrix} \right\| \le \varepsilon_2, \tag{4}$$

where $\varepsilon_1, \varepsilon_2 \ge 0$. By comparing constraints (3) and (4) we can determine the s coordinates from which we would like the signal to be generated and exclude off-resonance.

The last factor we must consider in our RF pulse sequence is slew rate $W(t)$, also known as gradient rise time. This identifies the speed at which a magnetic gradient field can be ramped to different gradient field strengths [7]. As the signal generated by the RF pulse is dependent on the gradient waveform, higher slew rates allow for shorter measurement times. Also, the gradient field strength can not exceed particular values otherwise it may distort the signal being processed for imaging.

Thus, the gradient field strength and slew rate must be bounded, in which we have the constraints

$$|G(t)| \le G_{\text{max}}, \tag{5}$$

$$W(t) = \left| \frac{dG(t)}{dt} \right| \le W_{\text{max}}. \tag{6}$$

Combining equations (1) – (6), we obtain the following nonlinear optimization problem

$$\min \text{SAR} = \int_0^T b_x^2(t) + b_y^2(t)dt, \tag{7}$$

subject to,

$$\frac{d\overrightarrow{M}(t,s)}{dt} = \gamma \begin{bmatrix} 0 & -sG(t) & b_y(t) \\ sG(t) & 0 & -b_x(t) \\ -b_y(t) & b_x(t) & 0 \end{bmatrix} \overrightarrow{M}(t,s), \tag{8}$$

$$\left\| \begin{bmatrix} M_0\sin(\alpha) \\ 0 \\ M_0\cos(\alpha) \end{bmatrix} - \begin{bmatrix} M_x(T,s) \\ M_y(T,s) \\ M_z(T,s) \end{bmatrix} \right\| \le \varepsilon_1, \tag{9S_{in}}$$

$$\left\| \begin{bmatrix} 0 \\ 0 \\ M_0 \end{bmatrix} - \begin{bmatrix} M_x(T,s) \\ M_y(T,s) \\ M_z(T,s) \end{bmatrix} \right\| \le \varepsilon_2, \tag{10S_{out}}$$

$$|G(t)| \le G_{\text{max}}, \tag{11}$$

$$\left| \frac{dG(t)}{dt} \right| \le W_{\text{max}}, \tag{12}$$

$$M_x(0,s) = 0, \ M_y(0,s) = 0, \ M_z(0,s) = M_0, \tag{13}$$

where equations (7) – (13) hold for $\forall\, s \in S,\, t \in [0,T]$. One may note that depending on whether the voxels are in S_{in} or S_{out}, constraints (9S_{in}) or (10S_{out}) are applicable. Thus, the gVERSE model presented in (7) – (13) has various sources of implementation issues, as we will discuss in the next section.

3.1. *gVERSE Discretization*

By separating our specimen into coordinate positions we have ultimately created two dimensional segments that are similar to records in a record box, whereby $s \in S$ represents the plane of a particular position in the specimen. In this section we discretize S into coordinate positions $s_1, s_2, \ldots, s_n$, where n is the total number of slices. As S_{in} refers to the coordinate positions whose magnetization vectors have been tipped into the transverse plane by an RF pulse, we can now define the finite band of particular coordinate positions in S_{in}. Thus, the coordinate positions corresponding to $s_k, \ldots, s_{k+\delta}$ will represent the voxels in S_{in}, where $1 < k \le k + \delta < n$, $\delta \ge 0$ and $k, \delta \in \mathbb{Z}$. The coordinate positions that are not excited in the transverse plane, those which belong to S_{out}, will consist of the remaining coordinate positions. Therefore, $S_{\text{out}} = s_1, \ldots, s_{k-1}, s_{(k+\delta)+1}, \ldots, s_n$. Figure 5 provides an illustration of how magnetization vectors for coordinate positions $s_i \in S, \forall\ i = 1, \ldots, n$ are separated into those that have been tipped into the transverse plane, and those that have not. In addition, one should note
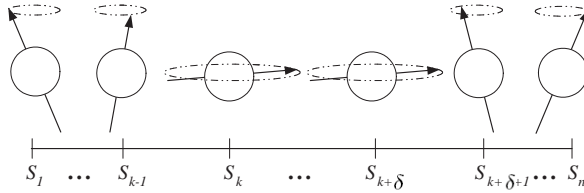

Fig. 5. Discretizing magnetization vectors into coordinate positions S_{in} and S_{out}.

that we have only discretized with respect to coordinate positions $s_i \in S$ and not with respect to time t. We next define the first coordinate position in S_{in} as $\underline{s}$ and the last position as $\overline{s}$. Thus, we have $\underline{s} = s_k$ and $\overline{s} = s_{k+\delta}$, and the coordinate positions in the slice become $S_{\text{in}} := [\underline{s}, \overline{s}]$. Conversely, the position where RF stimulation is a minimum and closest to $\underline{s}$, but in S_{out} (towards the direction of s_1) will be defined as $\underline{s}_l$. The same will be done for $\overline{s}_u$, the position closest to $\overline{s}$ that is in S_{out} (towards the direction of s_n). Therefore, $\underline{s}_l = s_{k-1}$ and $\overline{s}_u = s_{(k+\delta)+1}$, and $S_{\text{out}} := [s_1, \underline{s}_l] \cup [\overline{s}_u, s_n]$. As shown in Figure 5, S_{in} is located between the two subintervals of S_{out}, where $s_i \in S_{\text{in}}$ is centered around 0, leaving S_{out} subintervals, $[s_1, \underline{s}_l] < 0$ and $[\overline{s}_u, s_n] > 0$. In addition, coordinate positions that reside in $[s_1, \underline{s}_l]$ and $[\overline{s}_u, s_n]$ have symmetry. Hence, the length of these subintervals are equivalent, $s_{k-1} - s_1 = s_n - s_{(k+\delta)+1}$,

and the difference between respective coordinate positions are equal to one another such that,

$$
\begin{aligned}
s_2 - s_1 &= s_n - s_{n-1} \\
s_3 - s_2 &= s_{n-1} - s_{n-2} \\
&\vdots \qquad\qquad \vdots \\
s_{k-1} - s_{k-2} &= s_{(k+\delta)+2} - s_{(k+\delta)+1}.
\end{aligned} \tag{14}
$$

Also note that the discretization points, s_i, within any interval $[s_1, \underline{s}_l]$, $[\underline{s}, \overline{s}]$ or $[\overline{s}_u, s_n]$ are not necessarily uniformly distributed. For instance, more coordinate positions may be positioned closer to the boundaries of S_{in} and S_{out}. However, the distance between $(\underline{s}_l, \underline{s})$ and $(\overline{s}, \overline{s}_u)$ will be much larger in comparison to other increments of s_i. This is typically the area where off-resonance resides. As mentioned earlier, off-resonance disrupts pulse sequences and distorts MR imaging signals. Thus, we define tolerance gaps S_0 of finite length between $(\underline{s}_l, \underline{s})$ and $(\overline{s}, \overline{s}_u)$. Hence, the set S can now be partitioned into $S_{\text{in}} \cup S_{\text{out}} \cup S_0$, where the sequencing of the intervals are $S_{\text{out}}, S_0, S_{\text{in}}, S_0, S_{\text{out}}$.

4. Implementation

We now adapt the model described in the previous section to the forms of input accepted by Sparse Optimal Control Software (SOCS) and AMPL (the modeling language used to define the problem for the solver MINOS).

4.1. *SOCS Implementation*

The gVERSE model defined in the previous section proved to be a difficult NLP problem to solve, hence, Sparse Optimal Control Software (SOCS) from The Boeing Company was employed for this task. In this section, we will highlight the critical steps taken in converting the NLP from (7) – (13) into an optimal control problem. An optimal control problem is simply an infinite-dimensional extension of an NLP problem. In fact, practical methods for solving optimal control problems require iterations with a finite set of variables and constraints [3]. Typically, optimal control problems are formulated as a collection of state, control, and independent variables. By definition, state variables collectively capture the trajectory of the system, whereas control variables determine the course of the process [9]. For the gVERSE pulse problem the state and control variables are defined within the dynamics of the system.

Thus, for a problem with n slices, the state variables are defined by a $t(3n+1)$ dimensional state vector

$$\Omega(t) = [M_x(t, s_1), M_y(t, s_1), M_z(t, s_1),$$
$$\ldots, M_x(t, s_n), M_y(t, s_n), M_z(t, s_n), G(t)]^T$$

where $\Omega(t) \in \mathbb{R}^{3n+1}$. Similarly, the three dimensional control vector is

$$\Phi(t) = [b_x(t), b_y(t), W(t)]^T$$

with $\Phi(t) \in \mathbb{R}^3$. Subsequently, for any gVERSE pulse problem we solve, the total number of state and control variables are $t(3n+4)$. Our system is governed by differential equation (8) and slew rate, where for $i = 1, \ldots, n$ we have

$$\frac{dM_x(t, s_i)}{dt} = \gamma[-s_i G(t) M_y(t, s_i) + b_y(t) M_z(t, s_i)], \tag{15}$$

$$\frac{dM_y(t, s_i)}{dt} = \gamma[s_i G(t) M_x(t, s_i) - b_x(t) M_z(t, s_i)], \tag{16}$$

$$\frac{dM_z(t, s_i)}{dt} = \gamma[-b_y(t) M_x(t, s_i) + b_x(t) M_y(t, s_i)], \tag{17}$$

$$\frac{dG(t)}{dt} = W(t). \tag{18}$$

This can then be represented as a function of state and control variables, namely

$$f\big(\Omega(t), \Phi(t)\big) = \begin{bmatrix} \frac{dM_x(t,s_1)}{dt} \\[2mm] \frac{dM_y(t,s_1)}{dt} \\[2mm] \frac{dM_z(t,s_1)}{dt} \\[2mm] \vdots \\[2mm] \frac{dM_x(t,s_n)}{dt} \\[2mm] \frac{dM_y(t,s_n)}{dt} \\[2mm] \frac{dM_z(t,s_n)}{dt} \\[2mm] \frac{dG(t)}{dt} \end{bmatrix}, \tag{19}$$

where $f\big(\Omega(t), \Phi(t)\big)$ is a $t(3n+1)$ dimensional vector. In addition, the solution must also satisfy path constraints $G(t)$ and $W(t)$. For our problem bounds can be imposed on the state and control variables,

$$-G_{\max} \le G(t) \le G_{\max} \tag{20}$$
$$-W_{\max} \le W(t) \le W_{\max}, \tag{21}$$

which pertains to constraints (11) and (12), respectively. Therefore, we will define our path constraints by the vector

$$\Psi\big(\Omega(t), \Phi(t)\big) = \begin{bmatrix} G(t) \\ W(t) \end{bmatrix}, \tag{22}$$

which satisfies

$$\Psi_L \le \Psi\big(\Omega(t), \Phi(t)\big) \le \Psi_U, \tag{23}$$

where

$$-\Psi_L = \Psi_U = \begin{bmatrix} G_{\max} \\ W_{\max} \end{bmatrix}.$$

In anticipation of finding an optimal solution, boundary conditions define the values of particular state variables at the start and end time of our evaluation. This allows the value of the dynamic variables at the beginning and end of our time interval to be pre-defined [3]. Thus, the initial conditions at the start of the time interval, $t = 0$, are

$$M_x(0, s_i) = 0, \tag{24}$$
$$M_y(0, s_i) = 0, \tag{25}$$
$$M_z(0, s_i) = M_0, \tag{26}$$

again for $i = 1, \ldots, n$. Hence, the values from (24) – (26) are entered into $\Omega(0)$ at the beginning of our evaluation. Terminal conditions that must be satisfied at the end of the time interval are different for magnetization vectors in S_{in}, than for those in S_{out}. As depicted in constraints ($9S_{\text{in}}$) and ($10S_{\text{out}}$), at the end of our time interval $t = T$, the terminal condition for the voxels $s_i \in S_{\text{in}}$ are

$$-\varepsilon_1 \le \begin{bmatrix} M_0\sin(\alpha) \\ 0 \\ M_0\cos(\alpha) \end{bmatrix} - \begin{bmatrix} M_x(T, s_i) \\ M_y(T, s_i) \\ M_z(T, s_i) \end{bmatrix} \le \varepsilon_1. \tag{27}$$

Whereas, for voxels $s_i \in S_{\text{out}}$, we have the following terminal condition

$$-\varepsilon_2 \le \begin{bmatrix} 0 \\ 0 \\ M_0 \end{bmatrix} - \begin{bmatrix} M_x(T, s_i) \\ M_y(T, s_i) \\ M_z(T, s_i) \end{bmatrix} \le \varepsilon_2. \tag{28}$$

Therefore, the values for (27) and (28) are entered into $\Omega(T)$ and the boundary conditions for the gVERSE pulse problem are expressed by

$$\psi_L \le \psi\big(\Omega(t), \Phi(t)\big) \le \psi_U, \tag{29}$$

where ψ_L and ψ_U contain the respective initial and terminal condition values found in (24) – (28). Note that equality constraints can be imposed by simply setting upper and lower bounds equal to one another, i.e. $\psi_L = \psi_U$. Finally, the objective function to be minimized will be expressed as

$$\int_0^T w\big(\Phi(t)\big)\, dt = \int_0^T b_x^2(t) + b_y^2(t)\, dt, \qquad (30)$$

where $w\big(\Phi(t)\big)$ is known as the quadrature function in optimal control literature [4]. Collectively, we refer to the functions evaluated during the time interval as

$$F(t) = \begin{bmatrix} f\big(\Omega(t), \Phi(t)\big) \\ \Psi\big(\Omega(t), \Phi(t)\big) \\ w\big(\Phi(t)\big) \end{bmatrix}, \qquad (31)$$

the vector of continuous functions, however, boundary conditions evaluated at specific points are referred to as point functions [4]. Therefore, the solution to the optimal control problem requires

$$J(t) = \int_0^T w\big(\Phi(t)\big)\, dt \qquad (32)$$

to be minimized. Once the explicit details of the optimal control formulation have been established, it is then possible to solve the gVERSE pulse problem after the independent time variable has been discretized. Thus, time t is divided into N discretization points over the interval $[0, T]$, including the end points. Hence, the time discretizations are as follows:

$$0 = t_1 < t_2 < ... < T = t_N.$$

For more information on how an NLP is transformed into an optimal control problem the reader may consult [3,**?**,**?**].

Finally, we address the important subroutines and functions that were used in finding the solution to our optimal control problem. SOCS possesses powerful tools that can evaluate the gVERSE nonlinear constraint derivatives and the integral in the objective function. For a more detailed description of all the defaults and built in functions that SOCS contains one can refer to [4]. The key functions employed to solve the gVERSE problem are as follows:
HDSOCS
The subroutine HDSOCS is a powerful optimal control

routine provided by SOCS that was called to determine the $t(3n + 4)$ dimensional control and state vectors to minimize

$$J(\mathbf{x}) = \theta(\mathbf{x}) + \sum_{j=0}^T \left(\int_0^{t_j} w(\Phi(t_j))\, dt_j \right). \qquad (33)$$

HDSOCS was the central subroutine in the gVERSE pulse program, all other routines were eventually passed to HDSOCS in finding the optimal solution.
ODEINP
An important subroutine that must be present in HDSOCS is one that sequentially defines the variables and parameters involved in the optimal control problem. The generic name for this routine, which can be found in the SOCS manual [4], is ODEINP. This subroutine declares the gVERSE pulse variables, the number of time discretizations, the number of continuous and discrete user defined functions, the transcription method used to solve the problem, and other parameters used in locating the optimal solution. To solve the gVERSE pulse problem we utilized a Trapezoidal transcription method, which proved to provide the best results when compared to the other methods supplied by SOCS. Also, within this routine the user is required to assign certain values to particular functions defined within the software that ensures the problem is minimized.

ODERHS
HDSOCS also requires a subroutine known as ODERHS that supplies the quadrature function, $w(\Phi(t_j))$, and the dynamic variables implemented in the array $f(t_j, \hat{n})$, shown above. This subroutine was carefully implemented as it was called many times by SOCS during computation.

ODEPTF
The last important subroutine is ODEPTF, which is responsible for the terminal constraints outlined in the algorithm. This subroutine sets the appropriate terminal conditions for vectors in S_{in} and S_{out} to be relayed to HDSOCS.

Finally, a subroutine that initializes the data, assigns values for s_i positions, and separates them into S_{in} and S_{out} was also included in the implementation. This initialization subroutine has the capacity to input values for each time discretization point in what SOCS calls a guess function. With regards to the overall functionality of SOCS, although it is one of the most competitive NLP solvers, it is very difficult to use. For exam-

ple, defining the state and control variables in ODEINP have to be precisely ordered and counted. As well, to set up the quadrature objective, values are given to specific functions in SOCS that depend on how the model is formulated. Hence, careful planing on how to arrange the algorithms in your program is critical. For more detail on other routines and declarations necessary to the functionality of SOCS one can consult the SOCS manual [4].

4.2. *AMPL–MINOS Implementation Issues*

The results using SOCS optimal control software was compared to a well know NLP solver, AMPL–MINOS. Unlike SOCS, AMPL does not have built in functions that can evaluate integrals and derivatives. We used standard techniques to handle these areas of the gVERSE model and address them in this section. To begin, the objective function was calculated using a Riemann sum

$$\int_0^T b_x^2(t) + b_y^2(t)dt = \lim_{n=\infty} \frac{T-0}{n} \sum_{i=0}^n b_x^2(i) + b_y^2(i),$$

(34)

where i was uniformly distributed over the interval and for the implementation $n < \infty$, hence (34) becomes an approximation. Next we address the methods used to evaluate the derivatives found in the constraints. The Bloch equation

$$\frac{d\overrightarrow{M}(t,s)}{dt} = \gamma \begin{bmatrix} 0 & -sG(t) & b_y(t) \\ sG(t) & 0 & -b_x(t) \\ -b_y(t) & b_x(t) & 0 \end{bmatrix} \overrightarrow{M}(t,s),$$

(35)

becomes

$$\frac{dM_x(t,s_i)}{dt} = \gamma[-s_iG(t)M_y(t,s_i) + b_y(t)M_z(t,s_i)],$$

(36)

$$\frac{dM_y(t,s_i)}{dt} = \gamma[s_iG(t)M_x(t,s_i) - b_x(t)M_z(t,s_i)],$$

(37)

$$\frac{dM_z(t,s_i)}{dt} = \gamma[-b_y(t)M_x(t,s_i) + b_x(t)M_y(t,s_i)],$$

(38)

after expanding (35). For (36) – (38) a number of different integrating techniques can be employed, in which we tested a number of them and report the best results in the next section. Some of the techniques used include

a Taylor approximation, Multi-step approximation, up to symbolic integration over a time step. As an example, using a first order Taylor approximation about M_0 we have

$$M_x(t,s_i) \approx M_x(0,s_i) + \frac{dM_x(t,s_i)}{dt}(t - M_x(0,s_i))$$

(39)

$$= 0 + \gamma[-s_iG(t)M_y(t=0,s_i) + b_y(t)M_z(t=0,s_i)](t-0)$$

(40)

$$= \gamma[-s_iG(t)M_y(0,s_i) + b_y(t)M_z(0,s_i)]t,$$

(41)

and similarly

$$M_y(t,s_i) \approx \gamma[s_iG(t)M_x(0,s_i) - b_x(t)M_z(0,s_i)]t,$$

(42)

$$M_z(t,s_i) \approx 1 + \gamma[-b_y(t)M_x(0,s_i) + b_x(t)M_y(0,s_i)](t-1).$$

(43)

Thus, this constraint would be used in place of (8) for the AMPL implementation $\forall\, t \in [0,T]$. If a multi-step approximation is used then (41) – (43) becomes

$$M_x(t+1,s_i) \approx M_x(t,s_i) + h(\gamma[-s_iG(t)M_y(t,s_i) + b_y(t)M_z(t,s_i)]),$$

(44)

$$M_y(t+1,s_i) \approx M_y(t+1,s_i) + h(\gamma[s_iG(t)M_x(t,s_i) - b_x(t)M_z(t,s_i)]),$$

(45)

$$M_z(t+1,s_i) \approx M_z(t,s_i) + h(\gamma[-b_y(t)M_x(t,s_i) + b_x(t)M_y(t,s_i)]),$$

(46)

$\forall\, t \in [0,T]$, where $h \in (0,1)$ is a user defined step size that is typically set to 0.5 for our comparisons. The Bloch equations without relaxation can be solved analytically, but the resulting expression is highly non-linear. This changes one type of complexity for another. Finally, the constraint on Slew rate, namely

$$\left| \frac{dG(t)}{dt} \right| \leq W_{\max},$$

(47)

may be evaluated using the techniques mentioned above. However, since Slew rate bounds the slope of our gradient function, the following constraint

$$\left| \frac{G(t+1) - G(t)}{(t+1) - t} \right| \leq W_{\max}$$

(48)

may also be used in place of (12). Using the techniques presented in this section, the gVERSE model was then implemented and solved using AMPL–MINOS.

4.3. *Slice Assignment*

In the gVERSE model of Section 3.1., S was discretized into coordinate positions $s_1, s_2, \ldots, s_n$ and partitioned into the sets S_{in} and S_{out}. The coordinate positions in S_{in} were bounded by $[\underline{s}, \overline{s}]$ and S_{out} was composed of coordinate positions in $[s_1, \underline{s}_l]$ and $[\overline{s}_u, s_n]$. More specifically, $\underline{s}_l = s_{k-1}$, $\underline{s} = s_k$, $\overline{s} = s_{k+\delta}$ and $\overline{s}_u = s_{k+\delta+1}$ for $1 < k \leq k + \delta < n$ and $\delta \geq 0$. Thus, for an application with n slices, each $s_i \in S$ was given a scalar value defined by

$$s_i = \begin{cases} \underline{\beta} + \rho_1(i) & i \leq k - 1, \\ \beta + \rho_2(i) & k \leq i \leq k + \delta, \\ \overline{\beta} + \rho_3(i) & i \geq (k + \delta) + 1, \end{cases} \quad (49)$$

where $\underline{\beta}, \beta, \overline{\beta} \in \mathbb{R}$. In order to include the off-resonance characteristics found between $(\underline{s}_l, \underline{s})$ and $(\overline{s}, \overline{s}_u)$ the piecewise function in (49) is designed such that $\underline{\beta} + \rho_1(k - 1) < \beta \leq \beta + \rho_2(k + \delta) < \overline{\beta}$. Also, $\rho_1(i), \rho_2(i), \rho_3(i)$ are strictly monotonically increasing functions that can uniformly or randomly disperse increments of s_i. As stated in Section 3.1., the subinterval $[\underline{s}, \overline{s}]$ is intended to be centered around 0, and hence, β is chosen such that $\beta + \rho_2(i)$ has the same features for $k \leq i \leq k + \delta$. Also, the values $\underline{\beta} < 0$ and $\overline{\beta} > 0$ are assigned such that the positions $\underline{\beta} + \rho_1(i)$ for $i \leq k - 1$ and $\overline{\beta} + \rho_3(i)$ for $i \geq (k + \delta) + 1$ are symmetric with respect to each other, as shown in equation (14). By construction, $\beta + \rho_2(i)$ will contain the values for the magnetization vectors in S_{in}, whereas $\underline{\beta} + \rho_1(i)$ and $\overline{\beta} + \rho_3(i)$ will control the $s_i \in S_{\text{out}}$ values. The initial positions $\underline{\beta}, \beta, \overline{\beta}$ for this piecewise step function will be chosen depending on how many slices n we have, and how far we would like to disperse our RF pulse. For example, generally we would assign values such that $\underline{\beta} \approx s_1$, $\beta \approx s_k$ and $\overline{\beta} \approx s_{(k+\delta)+1}$. Also notice, we can set the distance between $\underline{\beta} + \rho_1(k - 1) < \beta$ and $\beta + \rho_2(k + \delta) < \overline{\beta}$ (S_0) to be as large or as small as we like. Thus, potentially controlling the negative imaging effects described in Section 3., which are experienced by off-resonance magnetization vectors. After the slices are separated into the sets S_{in} and S_{out} with appropriate values, they are ready to be evaluated within constraints (8) – (13). As mentioned, at $t_1 = 0$

the values of $M_x(0, s_i)$, $M_y(0, s_i)$, and $M_z(0, s_i)$ are initialized for $i = 1, \ldots, n$ in an input routine.

5. Computational Results

The gVERSE pulse was designed to minimize MRI SAR levels, however, in doing so a complex mathematical model was developed that challenges most software packages. In the previous section we highlighted different implementation issues between the two software packages that may be used to solve the model presented in (7) – (13). Using the SOCS SQP based optimal control software package and AMPL–MINOS the gVERSE RF pulse results are presented in this section. The number of decision variables in the problem is $N(3n + 4)$, where n is the total number of slices and N is the total number of time discretization points. For our comparison we used 15 slices and over 200 time evaluation points, in which SOCS has the capacity to increase this amount upon implementation. This pushed the softwares to their limits as memory limitations became an issue when the variable count was increased. Nonetheless, the given variable number captures the essential features of the problem and provides a meaningful comparison between the softwares. After consulting the MRI literature, the following parameter values were set: $\gamma = 42.58$ Hz/mT, $G_{\text{max}} = 0.02$ mT/mm, and $W_{\text{max}} = 0.2$ mT/mm/ms, where Hz is Hertz, mm is millimeters, ms is milliseconds, and mT is millitelsa. Also, $\alpha = \pi/2$ such that the S_{in} magnetization vectors were fully tipped into the transverse plane with $\varepsilon_1, \varepsilon_2 = 0.1$ degrees of freedom. Finally, the magnitude of the initial magnetization vector for each coordinate position was set to $M_0 = 1.0$ spin density units.

5.1. *Fifteen Slice gVERSE Comparison*

The gVERSE 15 slice model accounted for the largest size problem that SOCS could solve. As the distance from $\underline{s}_l$ to $\underline{s}$ and $\overline{s}$ to $\overline{s}_u$ decreased the model became even more difficult to solve. For our computational comparisons we used moderate settings for the distances between these magnetization vectors. To ensure the symmetric structure of the problem was maintained, the three middle magnetization vectors were part of S_{in} and the rest were included in S_{out}. Therefore, coordinate positions $\{s_7, s_8, s_9\} \in S_{\text{in}}$, while $\{s_1, \ldots, s_6, s_{10}, \ldots, s_{15}\} \in S_{\text{out}}$. An idea of how the magnetization vectors in the various coordinate positions should act is shown in Figure 6 and the
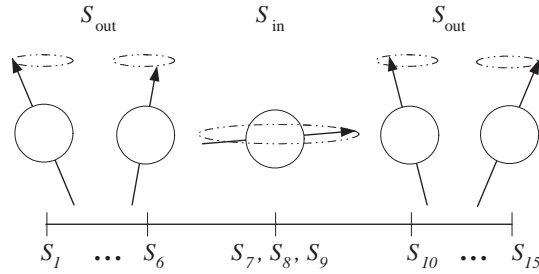
Fig. 6. The 15 coordinate positions of magnetization vectors $s_1, ..., s_{15}$ into S_{in} and S_{out}.

coordinate position values are as follows:

-30	-28	-26	-24	-22	-20	-0.2	0
s_1	s_2	s_3	s_4	s_5	s_6	s_7	s_8

0.2	20	22	24	26	28	30
s_9	s_{10}	s_{11}	s_{12}	s_{13}	s_{14}	s_{15}

where the positions are given in mm. The best results for the gVERSE 15 slice positions using SOCS and AMPL–MINOS are illustrated in Figures 7 – 11. Due to the symmetric structure of the problem, coordinate positions $s_1, \ldots, s_6$ and $s_{10}, \ldots, s_{15}$ were identical, as were s_7 and s_9. For this reason, we present the first eight coordinate positions. Figures 7 – 9 correspond to magnetization vectors in S_{out} and Figure 10 refers to the vectors in S_{in}. The resulting RF pulse and gradient waveforms are shown in Figure 11, where $b_x(t)$ was equal to zero for the SOCS results.

Examining the SOCS results in Figures 7 – 9 (a, c, e, g, i, k) one can observe the precession of the magnetization vectors in S_{out}. The starting point M_0 is within the range of the magnetization vectors precession, where it takes less than one full rotation to orbit uniformly. As the S_{out} vectors get closer to the RF pulse range (S_{in}) their orbiting radius increases. Hence, s_1, s_{15} and s_2, s_{14} magnetization vectors are tightly precessing versus that of s_5, s_{11} and s_6, s_{10}. This corresponds to expectations based on analytic constant coefficient solutions [11], thus, for the S_{out} magnetization vectors SOCS performs very well. Observing the S_{out} AMPL results in Figures 7 – 9 (b, d, f, h, j, l) one can see that precession is not evident. Although precession is not there, the data points do seem to get further apart from one another or are not as clustered as the magnetization vectors get closer to the RF pulse range. Hence, the AMPL results are not as strong as the SOCS results for the S_{out} vectors because they lack visually identifiable precession. This is not unexpected because SOCS has

the capacity to increase the number of time discretization points adaptively as a function of the controls, and therefore track the solution of the Bloch equation during time periods of large variation. For the magnetization vectors in S_{in}, Figure 10, the SOCS results – graphs (m, o) – smoothly tip into the transverse plane. Note that the model was designed in the rotating frame of reference, hence, these graphs should not show any rotation (refer to Section 3.). There are small differences between magnetization vectors s_7, s_9 (Figure 10 (m)) and s_8 (Figure 10 (o)), however, below 0.8 spin density units they act very similar. Also note that the vectors tip to just below 0.1 spin density units, as this was the upper bound set by ε_1. Again, SOCS has produced results that are very similar to expectations. The AMPL results are better for the S_{in} voxels than that of the S_{out}, with regards to magnetization vector behavior. In Figure 10 (n, p) the magnetization vectors tip into the transverse plane, however, the sharp projections seem to be somewhat unrealistic. As with the SOCS results, there are differences with respect to s_7, s_9 (Figure 10 (n)) and s_8 (Figure 10 (p)), where s_8 seems to be more smooth. In addition, the magnetization vectors triangular projection are more of a result of the integration method and low temporal resolution used, than the expected solution. Finally, Figure 11 presents the RF pulse and the accompanying gradient waveform. For the SOCS results the external magnetization components, $b_x(t)$ and $b_y(t)$, are constant and linear. As mentioned, $b_x(t)$ was zero and $b_y(t)$ is shown in Figure 11 (a). This is precisely what the gVERSE pulse was designed to do as our objective function optimized these two values. In the AMPL results, Figure 11 (b), $b_y(t)$ and $b_x(t)$ were constant for parts of the pulse but produced an uncommon triangular function. For both gradient waveforms in the SOCS and AMPL results, Figure 11 (c, d), the graphs are non-smooth functions and are predominantly negative functions. For the SOCS results the gradient function starts
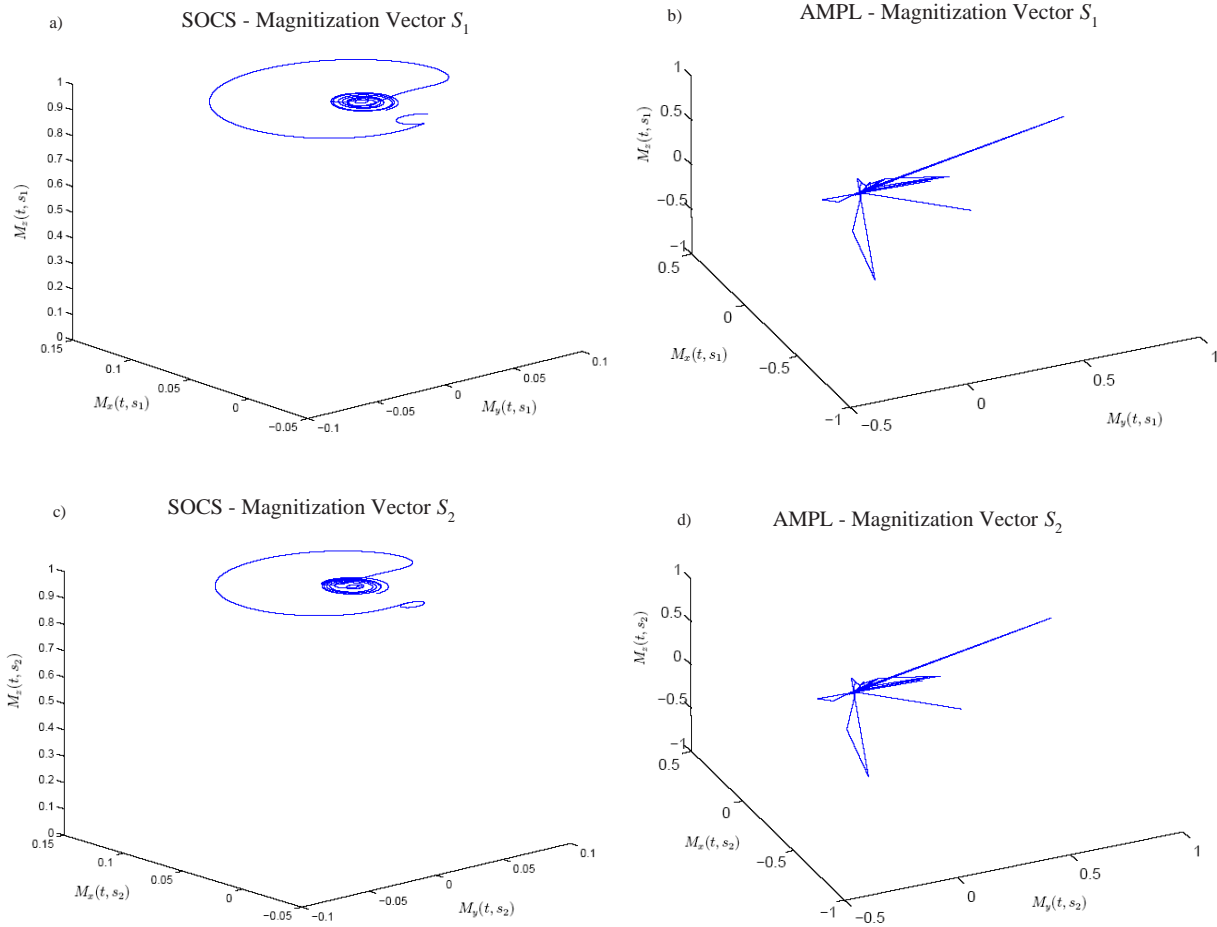
a) SOCS - Magnitization Vector S_1

b) AMPL - Magnitization Vector S_1

c) SOCS - Magnitization Vector S_2

d) AMPL - Magnitization Vector S_2

Fig. 7. Magnetization vectors corresponding to coordinate positions s_1, s_{15}: (a), (b) and s_2, s_{14}: (c), (d). SOCS results are shown in graphs (a) and (c), and AMPL–MINOS results in graphs (b) and (d).

off negative and ends up positive. This is quite the opposite to what is used in typical MRI sequences, however, as we will investigate in the next section it proves to be proficient. Of the two results, the AMPL sequence (Figure 11 (d)) has more smoother pieces than that of the SOCS (Figure 11 (c)), yet, either gradient sequence may be implemented using an MRI. The objective value for the SOCS computations was 0.0385 SAR units and for the AMPL computations it was 0.0006 SAR units. For comparison, the SAR value of a conventional RF SINC pulse is 0.5923 SAR units, hence, both optimal values were significantly below what is currently used.

5.2. *Signal Verification*

To obtain a better understanding of how the gVERSE pulse would perform in vivo we designed an MRI sim-

ulation. From the literature [10–13] one can find information on how the signal is mathematically amplified, digitized, and transformed to form a final image. The simulation was implemented in Matlab, where a 1D imaging coverage was used as shown in [1,15]. Using the gVERSE SOCS and AMPL RF pulse and gradient waveform results we conducted a number of MR imaging simulations over various tissues. We present one of the imaging results, for more examples the reader may refer to [15].

The MR signal generated by the RF pulse has a direct relationship with that of the tissues spin density. We used cerebrospinal fluid, which has a spin density value of 1.0. Also, the cerebrospinal fluid was placed on an angle as an MRI performance technique, shown in Figure
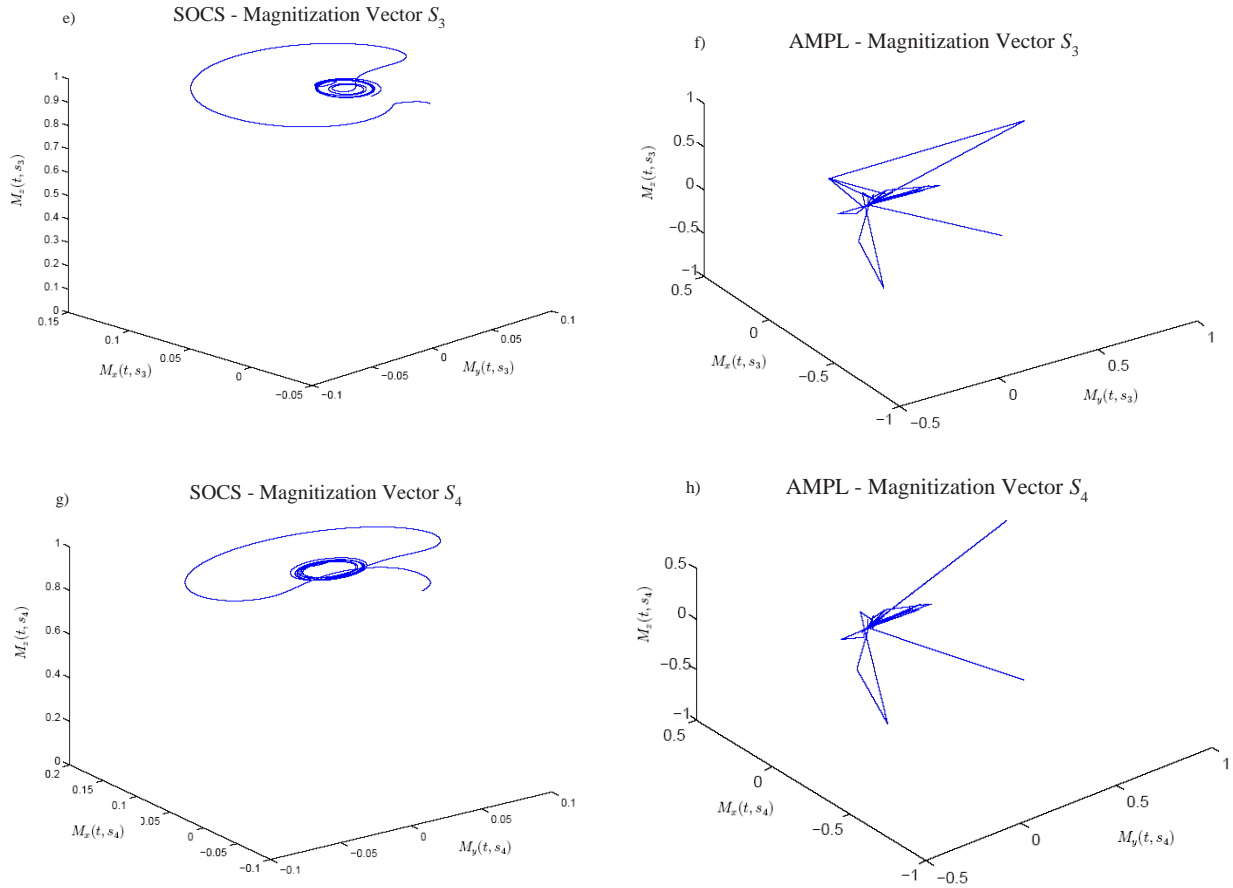
Fig. 8. Magnetization vectors corresponding to coordinate positions s_3, s_{13}: (e), (f) and s_4, s_{12}: (g), (h). SOCS results are shown in graphs (e) and (g), and AMPL–MINOS results in graphs (f) and (h).

12 (a). For the pulse to work as designed only the voxels in coordinate positions corresponding to S_{in} should produce a signal, which equates to a peak. Hence, only in this region should a reading be produced, any signal before or after this region would be accounted as noise and reduce the performance of the pulse. Figure 12 (b) is an illustration of an MR signal produced from a generic SINC pulse sequence when run through the simulation. The central peak in the signal represents when the pulse reaches the S_{in} region. Since discrete time points were used in our model the plot is not a smooth function, but in practice it would be. Figure 12 (c) is the signal reading when the gVERSE pulse is used with the SOCS results. As shown, the gVERSE pulse seems to have a larger central peak and less noise. The base of the signal in Figure 12 (c) is very representative to the voxels in S_{in} of the fluid, and the peak remains con-

stant throughout the duration of the signal. This would produce a high quality signal with more data points to process for imaging. The AMPL results do not produce a strong signal under the same conditions. In addition, as shown in Figure 12 (d), it is not as representative as the SOCS results with respect to when the voxels enter S_{in}, which was expected given the poor voxel results in the previous section.

6. Conclusions and Future Work

The gVERSE model was designed to reduce the SAR of RF pulses by maintaining a constant RF pulse strength ($\vec{B}_{rf}$ value) while generating high quality MR signals. The observations made in Section 5. deserve some additional reasoning and explanation. To begin,
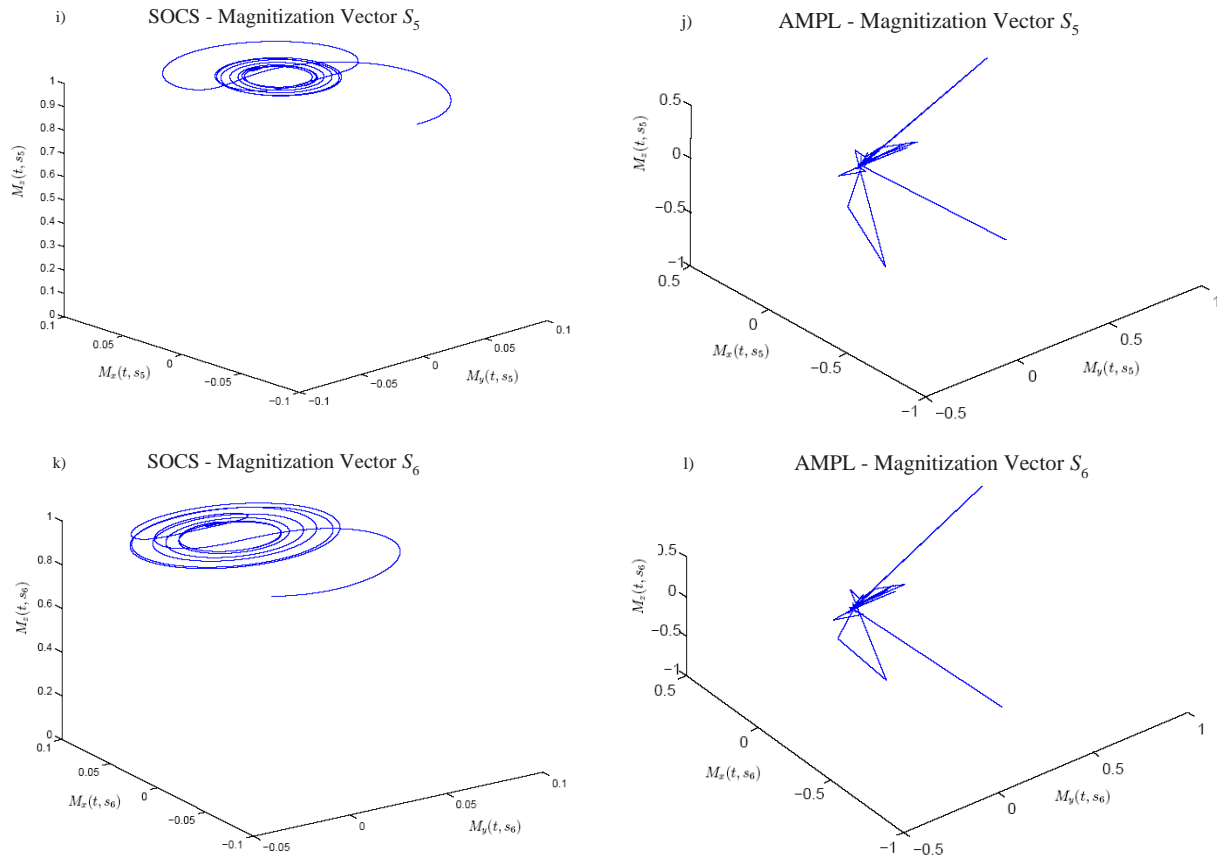
Fig. 9. Magnetization vectors corresponding to coordinate positions s_5, s_{11}: (i), (j) and s_6, s_{10}: (k), (l). SOCS results are shown in graphs (i) and (k), and AMPL–MINOS results in graphs (k) and (l).

the reader should understand that the symmetry displayed between coordinate position vectors in each of the result cases was precisely designed in the gVERSE model. The precession of the the magnetization vectors illustrated in the SOCS results, however, was not directly part of the gVERSE design, rather it was a consequence of the Bloch equation in constraint (8). Nonetheless, the precession shown in the SOCS results validated the design. This was not the case for the AMPL results, precession was not present in any of the graphs pertaining to S_{out}. Furthermore, investigating the precession of the magnetization vectors in the SOCS results, it was shown that they had a much tighter radial orbit towards the outer coordinate positions than those closer to $\underline{s}_l$ and $\overline{s}_u$. With regards to the magnetization vectors in S_{in}, the SOCS results were much more realistic than the AMPL cases. Finally, in terms of our optimal solution, which directly relates

to the level of SAR produced during the RF pluse sequence, both AMPL and SOCS were able to greatly reduce this value.

As the voxel behaviour of the SOCS solutions were very close to expectations, the RF pulse and gradient waveforms performed very well with regards to the MRI simulation. This was not the case for the AMPL-MINOS results, and the unrealistic voxel behaviour may have accounted for the poor signal readings. One should note that our AMPL implementation was based on general mathematical techniques. Analytic integration of the Bloch equations did not help. Some type of adaptive time stepping might have helped the AMPL results, but this would have required substantial programming and not been in the spirit of comparing the applicability and performance results of the two software packages. The most interesting part of the
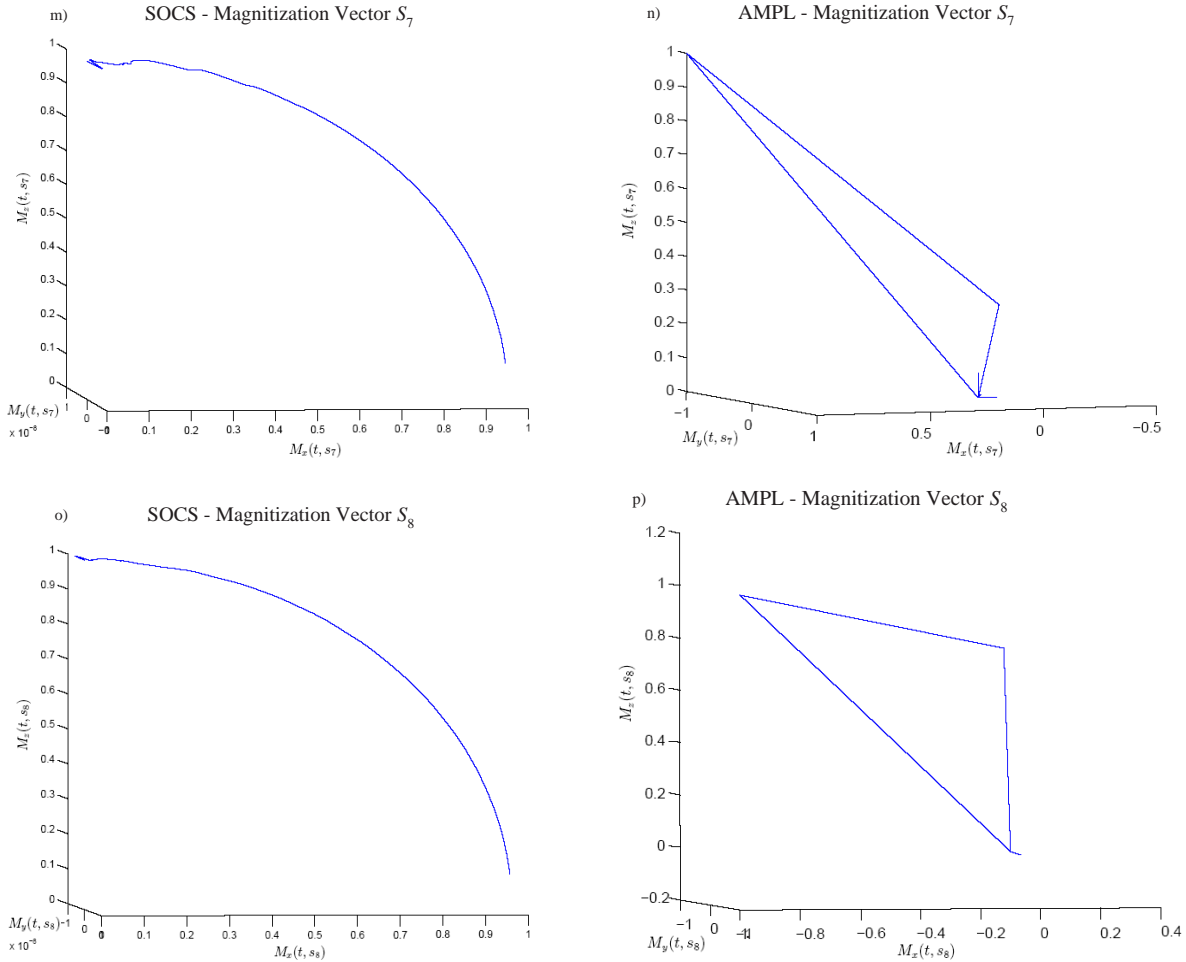
m)   SOCS - Magnetization Vector S_7

n)   AMPL - Magnetization Vector S_7

o)   SOCS - Magnetization Vector S_8

p)   AMPL - Magnetization Vector S_8

Fig. 10. Magnetization vectors corresponding to coordinate positions s_7, s_9: (m), (n) and s_8: (o), (p). SOCS results are shown in graphs (m) and (o), and AMPL–MINOS results in graphs (n) and (p).

gVERSE results was the gradient waveform. The RF pulse in our model was optimized such that this process returned a gradient waveform that would provide the appropriate spatial signal. In other words, in order to use the $b_x(t)$ and $b_y(t)$ pulse design, the accompanying gradient waveform would have to be imposed to acquire a useable signal. With regards to practical MR gradient waveforms, the AMPL results seem to be the easier of the two to implicate. However, regardless of the difficulty, recent improvements in gradient hardware will allow either gradient to be implemented, as mentioned in [8]. In addition, both results have similar features in the sense that they each started off negative and then ended up positive. As shown in Section 2., conventional gradient sequences usually have the op-

posite characteristics. In terms of our SOCS MRI simulation results, strong signal readings were produced using the gVERSE SOCS RF pulse sequence. For this reason, various MRI studies utilizing gVERSE pulses may be considered for future research developments.

In this paper, we investigated the different solutions produced by two competitive softwares. The SOCS and the AMPL results show that not only is the design of the RF pulse sequence important, but the software used to solve the NLP can have a profound effect on the quality of the solution. Although one may argue that SOCS has more features to accommodate the model presented in (7) – (13), even if a biased comparison was used, the AMPL tests using analytic solutions to the Bloch equa-
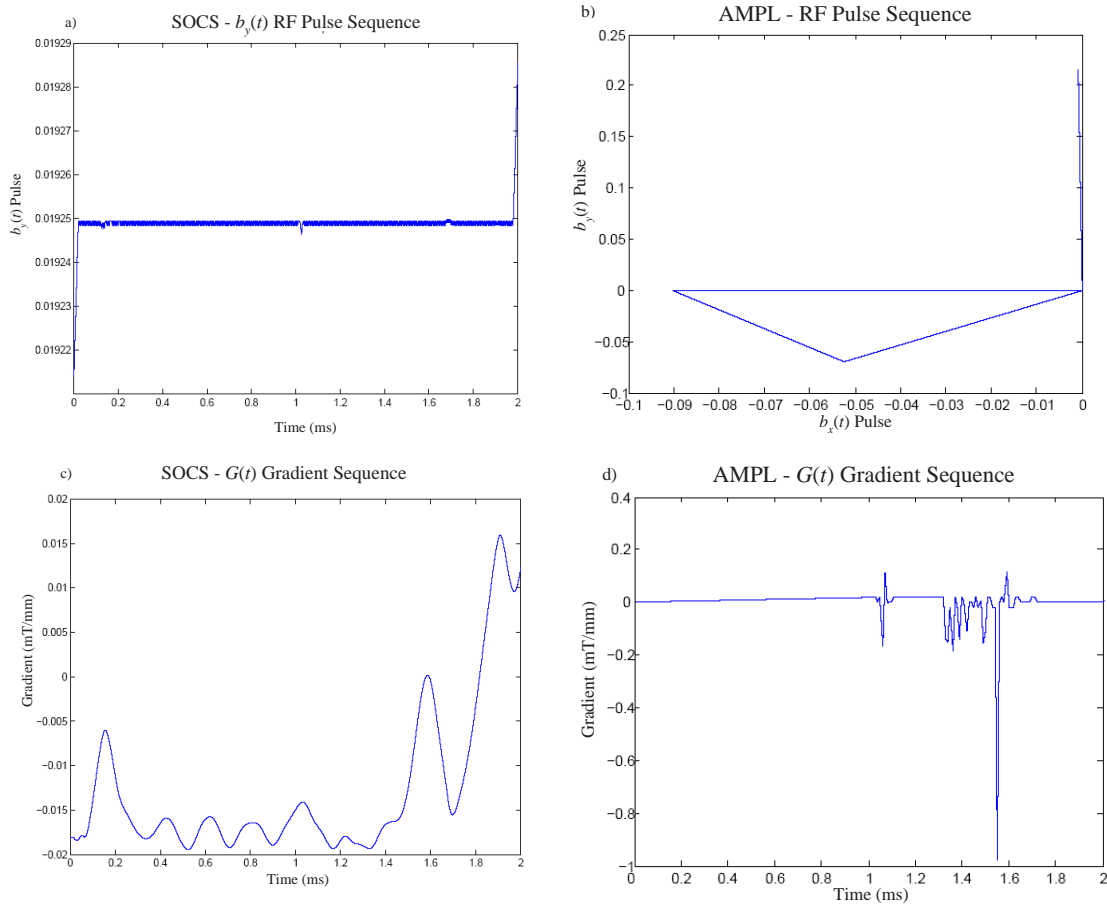
Fig. 11. External magnetization components presented in graphs (a) and (b), and gradient sequence $G(t)$ in graphs (c) and (d). SOCS results are shown in graphs (a) and (c), and AMPL–MINOS results in graphs (b) and (d).

tions and increasing the number of time steps to the final number of time steps reported by SOCS did not have any significant impact on the final results. Such additions resulted in substantially increased computation time without producing solutions containing the desired features (i.e. precession) apparent in the SOCS solutions. Again, while it is possible to implement adaptive time stepping and other features of SOCS in AMPL, this would involve substantial programming, and could not be considered as a comparison of the existing software packages. Also, in that case SOCS could also be improved by providing it with symbolic derivatives, or improving memory allocation to take advantage of the fact that the Bloch equations at different slice positions are independent, and can therefore reuse memory in their integration. Therefore, a few of the areas of interest for future investigations include:

- Solving the gVERSE problem using alternative NLP software than the ones presented;
- Designing a customized method to handle the coding obstacles presented in Section 4.2.;
- Including other aspects in the gVERSE model such as spin-lattice and spin-spin proton interactions;
- Applying the gVERSE pulse sequence to an MRI machine.

References

[1] C.K. Anand, S.J. Stoyan, T. Terlaky. The gVERSE RF Pulse: An Optimal Approach to MRI Pulse Design. Chapter in the text book: Simulation and Optimization of Complex Processes, *Springer*, New York (2008)

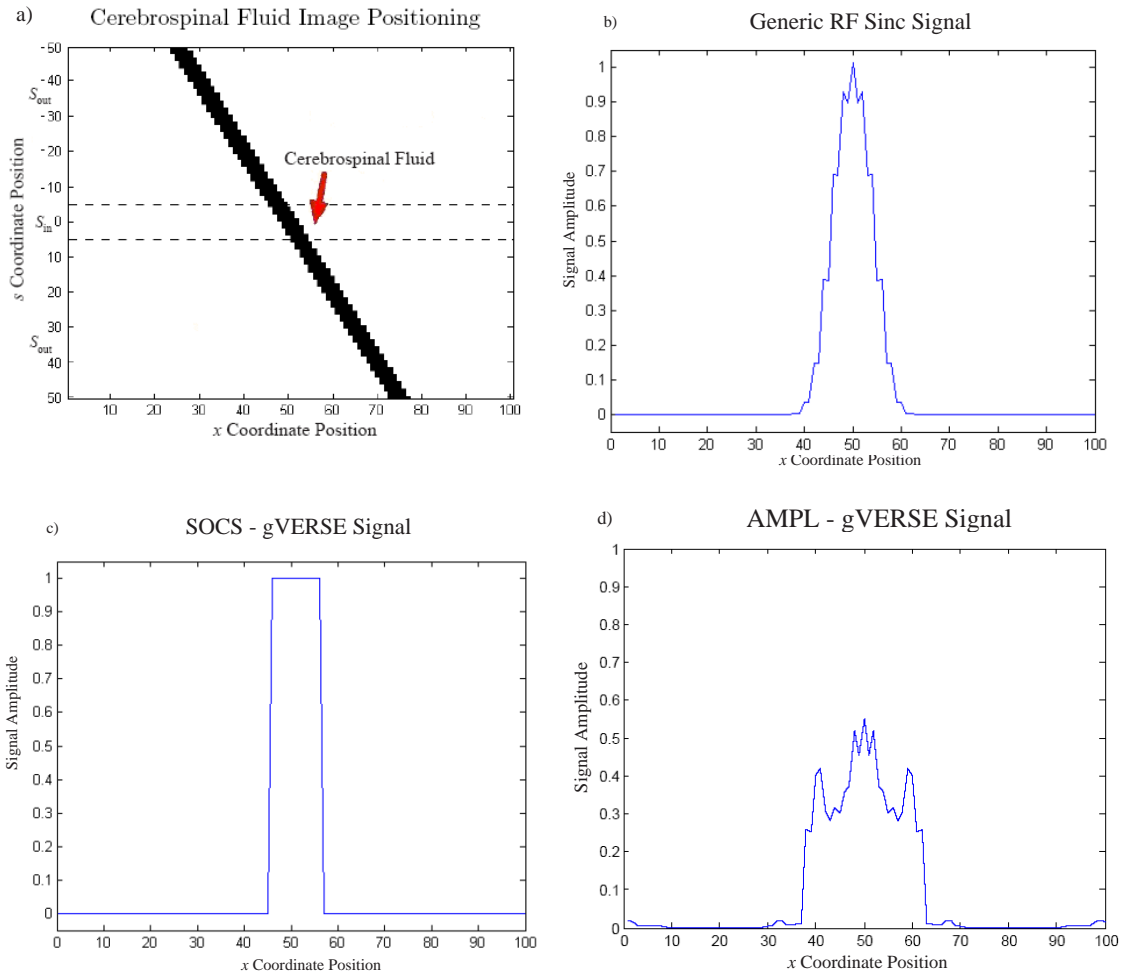[2] Bertsekas, D.P.: Nonlinear Programming. Athena Scientific, Belmont, Massachusetts (1995)

Fig. 12. The signal produced by an MRI simulation over a diagonal cerebrospinal fluid specimen (a), when a generic SINC RF pulse sequence is applied (b) and the gVERSE SOCS (c) and AMPL (d) results.

[3] Betts, J.T.: Practical Methods for Optimal Control Using Nonlinear Programming. Society for Industrial and Applied Mathematics, Philadelphia (2001), Second edition (2010)

[4] Betts, J.T., and Huffman, W.P.: Manual: Release 6.2 M and CT-TECH-01-014. The Boeing Company, PO Box 3707. Seattle, WA 98124-2207 (2001)

[5] Bushong, S.C.: Magnetic Resonance Imaging: Physical and Biological Principles. Mosby, Toronto, 2nd edition (1996)

[6] Conolly, S.M., Nishimura, D. G., and Macovski, A.: Optimal Control Solutoins to the Magnetic Resonace Selelctive Excitation Problem. IEEE Transacitons on Medical Imaging, MI-5, 106-115 (1986)

[7] Conolly, S.M., Glover, G., Nishimura, D.G., and Macovski, A.: Variable-Rate Selective Excitation. Journal of Magnetic Resonance, 78, 440-458 (1988)

[8] Hargreaves, B.A., Cunningham, C.H., Nishimura, D.G., and Conolly, S.M.: Variable-Rate Selective Excitation for Rapid MRI Sequences. Magnetic Resonance in Medicine, 52, 590597 (2004)

[9] Connors, M.M., and Teichroew, D.: Optimal Control of Dynamic Operations Research Models, International Textbook Company, Pennsylvania (1997)

[10] Curry, T.S., Dowdey, J.E., and Murry, R.C.: Christensen's Physics of Diagnostic Radiology. Lippincott Williams and Wilkins, New York, 4th edition (1990)

[11] Haacke, E.M., Brown, R.W., Thompson, M.R., and Venkatesan, R.: Magnetic Resonance Imaging: Physical Principles and Sequence Design, John Wiley and Sons, Toronto (1999)

[12] Liang, Z.P., and Lauterbur, P.C.: Principles of Magnetic

Resonance Imaging: A Signal Processing Perspective. IEEE Press, New York, New York (2001)

[13] Nishimura, D.G.: Principles of Magnetic Resonance Imaging. Department of Electrical Engineering, Stanford University, San Francisco (1996)

[14] Shen, J.: Delayed-Focus Pulses Obtimized Using Simulated Annealing. Journal of Magnetic Resonance, 149, 234-238 (2001)

[15] Stoyan, S.J.: Variable Rate Selective Excitation RF Pulse

in MRI. M.Sc. Thesis: McMaster University, Hamilton (2004)

[16] Ulloa, J.L., Guarini, M., and Irarrazaval, P.: Chebyshev Series for Designing RF Pulses Employing an Optimal Control Approach. IEEE Transacitons on Medical Imaging, 23, 1445-1452 (2004)

[17] Wu, X.L., Xu, P., and Freeman, R.: Delayed-Focus Pulses for Magnetic Resonace Imaging: An Evolutionary Approach. Magnetic Resonance Medicine, 20, 165-170 (1991)